


Hit-Time and Hit-Position Reconstruction in Strips of Plastic Scintillators Using Multithreshold Readouts

N. G. Sharma , M. Silarski, J. Chhokar, E. Czerwiński, C. Curceanu, K. Dulski, K. Farbaniec, A. Gajos, R. Del Grande, M. Gorgol, B. C. Hiesmayr, B. Jasińska, K. Kacprzak, Ł. Kapłon, D. Kisielewska, K. Klimaszewski, G. Korcyl, P. Kowalski, N. Krawczyk, W. Krzemień, T. Kozik, E. Kubicz, M. Mohammed, Sz. Niedźwiecki, M. Pałka, M. Pawlik-Niedźwiecka, L. Raczyński, J. Raj, S. Sharma, S. Shivani, R. Y. Shopa, M. Skurzok, W. Wiślicki, B. Zgardzińska, and P. Moskal

Abstract—In this article, a new method for the reconstruction of hit-position and hit-time of photons in long scintillator detectors is investigated. This article is motivated by the recent development of the positron emission tomography scanners based on plastic scintillators. The proposed method constitutes a new way of signal processing in multivoltage-technique. It is based on the determination of the degree of similarity between the registered signals and the synchronized model signals stored in a library. The library was established for a set of well-defined hit-positions along the length of the scintillator. The Mahalanobis distance was used as a measure of similarity between the two compared signals. The method was validated on the experimental data measured using two-strips J-PET prototype with

dimensions of $5 \times 9 \times 300$ mm³. The obtained time-of-flight (TOF) and spatial resolutions amount to 325 ps (FWHM) and 25 mm (FWHM), respectively. The TOF resolution was also compared to the results of an analogous study done using the linear fitting method. The best TOF resolution was obtained with this method at four predefined threshold levels which was comparable to the resolution achieved from the Mahalanobis distance at two predefined threshold levels. Although the algorithm of the linear fitting method is much simpler to apply than the Mahalanobis method, the application of the Mahalanobis distance requires a lower number of applied threshold levels and, hence, decreases the costs of electronics used in PET scanner.

Index Terms—J-PET detector, Mahalanobis distance, medical imaging, spatial resolution, TOF resolution.

Manuscript received July 24, 2019; revised October 30, 2019 and January 7, 2020; accepted March 28, 2020. Date of publication April 28, 2020; date of current version September 2, 2020. This work was supported in part by the Polish National Center for Research and Development under Grant INNOTECH-K1/IN1/64/159174/NCBR/12, in part by the Foundation for Polish Science through the MPD and TEAM under Grant POIR.04.04.00-00-4204/17 programmes, in part by the National Science Centre of Poland under Grant 2016/21/B/ST2/01222 and Grant 2017/25/N/NZ1/00861, in part by the Ministry for Science and Higher Education under Grant 6673/IA/SP/2016, Grant 7150/E-338/SPUB/2017/1, and Grant 7150/E-338/M/2017, and in part by the Austrian Science Fund under Grant FWF-P26783 and DSC grants. (Corresponding author: N. G. Sharma.)

N. G. Sharma, M. Silarski, J. Chhokar, E. Czerwiński, K. Dulski, K. Farbaniec, A. Gajos, K. Kacprzak, Ł. Kapłon, D. Kisielewska, G. Korcyl, N. Krawczyk, T. Kozik, E. Kubicz, Sz. Niedźwiecki, M. Pałka, M. Pawlik-Niedźwiecka, J. Raj, S. Sharma, S. Shivani, M. Skurzok, and P. Moskal are with the Faculty of Physics, Astronomy and Applied Computer Science, Jagiellonian University, 30-348 Kraków, Poland (e-mail: pnp.neha@gmail.com).

C. Curceanu and R. Del Grande are with the INFN, Laboratori Nazionali di Frascati, 00044 Frascati, Italy.

M. Gorgol, B. Jasińska, and B. Zgardzińska are with the Institute of Physics, Maria Curie-Skłodowska University, 20-031 Lublin, Poland.

B. C. Hiesmayr is with the Faculty of Physics, University of Vienna, 1090 Vienna, Austria.

W. Krzemień is with the High Energy Physics Division, National Centre for Nuclear Research, 05-400 Otwock-Świerk, Poland.

K. Klimaszewski, P. Kowalski, L. Raczyński, R. Y. Shopa, and W. Wiślicki are with the Department of Complex Systems, National Centre for Nuclear Research, 05-400 Otwock-Świerk, Poland.

M. Mohammed is with the Faculty of Physics, Astronomy and Applied Computer Science, Jagiellonian University, 30-348 Kraków, Poland, and also with the Department of Physics, College of Education for Pure Sciences, University of Mosul, Mosul 41002, Iraq.

Color versions of one or more of the figures in this article are available online at <http://ieeexplore.ieee.org>.

Digital Object Identifier 10.1109/TRPMS.2020.2990621

2469-7311 © 2020 IEEE. Personal use is permitted, but republication/redistribution requires IEEE permission.

See <https://www.ieee.org/publications/rights/index.html> for more information.

I. INTRODUCTION

POSITRON emission tomography is a noninvasive imaging technique used in medical diagnostics. It uses a short-lived positron-emitting radioactive tracer which is injected into the patient's body. The density distribution of the tracer is determined by pairs of back-to-back gamma quanta registered by detectors surrounding the patient. Emission of gamma quanta occurs as a result of the annihilation of a positron with an electron present inside the patient's body. PET scanners available commercially use crystal scintillators as radiation detectors and they have an axial extent of about 17–25 cm [1], [2]. The time and spatial resolutions obtained by the best PET scanners are about 210–400 ps and 4.7–6 mm, respectively [1], [3].

One of the challenges in the PET tomography is to increase the axial extent. In current PET scanners roughly 85%–90% of the patient's body is outside of the field-of-view (FOV) of the scanner, hence, only 1% of pairs of coincidence photons emitted from the body are detected [1], [2], [4]. The extension of detector rings from 20-cm axial FOV to a 200-cm FOV would allow maximal detection of radiation emitted from the body and hence improve the sensitivity and signal-to-noise ratio. Furthermore, with improved sensitivity, the radiation dose needed for the whole body scan could be decreased which in turn will allow usage of short-lived radionuclides like ¹¹C.

The extension of axial FOV to total-body scan may also enable newly developed positronium imaging [5], [6]. To address this problem many new PET concepts have been proposed, like the lead-walled straw PET detector (LWS) [7], [8], the resistive plate chamber PET (RPC) [9], [10], axial geometry-based PET scanners [11], [12], and the EXPLORER total-body PET tomograph [13]–[15]. The J-PET scanner [16]–[20] constitutes another economical solution with large FOV, built out of plastic scintillators. The relatively low probability of annihilation photons detection with plastic scintillators can be overcome by using longer modules and more detection layers [21]. The axial arrangement of plastic strips allows placing the electronic readout system [22]–[25] outside of the detectors, with a great benefit for medical diagnostics since it enables simultaneous application of PET and CT, as well as PET and MRI. The later hybrid is already achieved also with the crystal-based PET/MRI systems [1].

This novel solution of long detection modules requires new optimization methods for the determination of the hit-time and the hit-position. There have been several attempts made so far to optimize the reconstruction [18], [26]–[30], however, in this article, we present another idea based on the fact that the shape of signals registered at the end of a plastic bar depends significantly on the position of interaction. The idea was realized in two steps: first, creation of library of synchronized model signals and second, reconstruction of hit-time and hit-position of annihilation gamma quanta. The reconstruction is based on the comparison between measured signal and signals from the library. As a measure of similarity a Mahalanobis distance is used which accounts for the uncertainties of the signals samplings and correlations between uncertainties. A similar method was already presented in [28] but with chi-square minimization function used as a measure of similarity. In this article, the first step is extended further with additional conditions of signal selection followed by the reconstruction method using Mahalanobis distance. The method, similarly as the one introduced in [28], requires application of the multivoltage-threshold (MVT) technique introduced and developed by [31]–[33]. The main motivation of the research presented in this article is to find out a measure of similarity which would enable to minimize the number of threshold used, and to facilitate more economical construction of PET modalities with long axial FOV.

This article is structured into four sections: first, the concept of the J-PET detector and the two strip J-PET prototype is briefly described. Then, the general idea behind the proposed reconstruction method including a description of signal processing is presented. In the next section, the realization and validation of the method is explained. Finally, the experimental results are presented and discussed.

II. J-PET DETECTOR

The J-PET scanner uses organic scintillators arranged axially (see Fig. 1) as a radiation detectors. Signals from each detection module are read out by a pair of photomultipliers (PMs) connected to the two ends of each strip, as shown in Fig. 2. Organic scintillators have a long light attenuation length

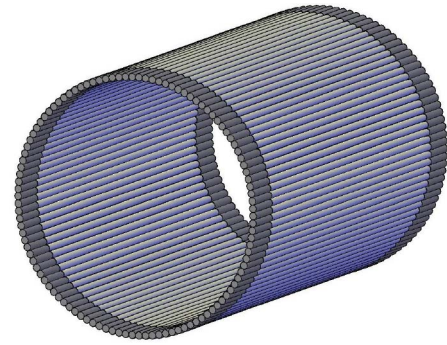


Fig. 1. Schematic arrangement of the detection modules providing large FOV used in the J-PET scanner. In the module all the scintillators are connected to a pair of PMs at both ends.

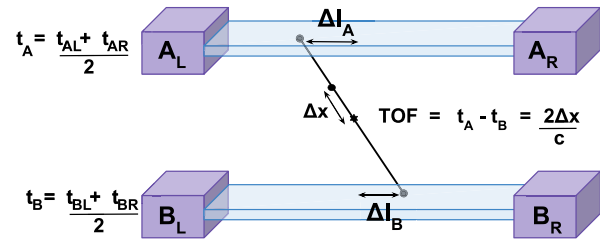


Fig. 2. Pictorial representation of the annihilation point reconstruction using the TOF method in the J-PET detector. t_{AL} and t_{AR} are the time values measured for signals obtained from left- and right-ended PMs of strip A at some predefined threshold levels and t_A is their average. Similarly, t_{BL} and t_{BR} are the time values of left and right signals obtained from strip B and t_B is the average. Δl_A and Δl_B are the distances of the hit-positions of photons within the scintillators A and B from their central positions, respectively. Δx is the distance along LOR between the point of annihilation and the center of LOR.

(in the order of 100 cm to 400 cm [34], [35]), in comparison to crystal scintillators (~ 10 cm [35]–[37]), which allows to make large diagnostic chambers from long scintillators strips. The annihilation gamma quanta with 511-keV energy interact in plastic scintillators predominantly via Compton scattering. The hit-position and hit-time of the annihilated photons can be determined from the arrival time information of signals detected by the PMs placed at each end of the detection module. Similarly, the position along the line-of-response (LOR) can be determined using time-of-flight (TOF) information, as shown in Fig. 2.

Fig. 3 shows typical signals obtained from a single detection module consisting of a plastic scintillator optically connected to a pair of PMs at three different irradiated positions with gamma quanta. As one can see the shape and amplitude of the signals vary with the interaction point of gamma quanta within the scintillator. The J-PET electronics used to process signals from the PMs enables to determine their widths and times at which they crossed the given reference voltages by means of multithreshold constant-level discriminators [22], [23]. A pictorial representation of signal sampling in voltage domain is shown in Fig. 4.

As mentioned above and illustrated in Fig. 3, in the J-PET scanner the shape and amplitude of signals strongly depend on the hit-position of gamma quanta in the strip. This dependency becomes stronger with increasing size of the scintillator and hence, influences the time and position resolution. Moreover,

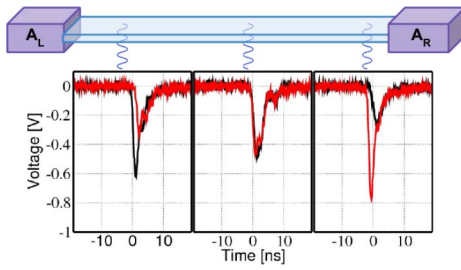


Fig. 3. Example of signals obtained at three different irradiated positions from a pair of PMs connected to the ends of a scintillator strip. Solid black and red lines represent the left and right signals measured by left (A_L) and right (A_R) PM, respectively. The measurements were conducted with BC-420 scintillators [36] and R9800 photomultipliers [38].

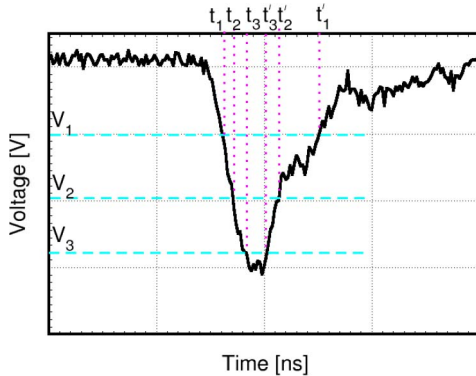


Fig. 4. Sampling of signal in the voltage domain at three defined voltages V_1 , V_2 , and V_3 as it is done by the J-PET electronics. As a result, in the presented example one obtains three time values measured at the leading (t_1 , t_2 , t_3) and three times values at the trailing edge (t'_1 , t'_2 , t'_3).

the final uncertainty in reconstruction of the annihilation point and herewith the performance of the PET-scanner depends strongly on the time resolution.

As it will be shown in next sections of this article, the strong change of signal shape along the scintillator strip can be utilized in optimizing the position and time of photons interaction. It is important to remark that a single event as a result of annihilation, refers to two signal curves in each strip, so in total of four signal curves. The reconstruction method which we propose was developed and optimized on the two strips J-PET prototype read out by a Serial Data Analyzer which provided full signals gathering. However, in order to, simulate the real J-PET tomograph electronics, we have emulated the sampling in the voltage domain [39]. In general, this reconstruction method can be used in other state-of-the-art scanners, which sample signals in voltage domain either by means of multithreshold constant-level discriminators or by means of constant-fraction discriminators. Here, it is worth noting that recently new methods for multivoltage sampling based on field-programmable gate arrays (FPGA) were developed [22]–[25], [40]–[44] for application in positron emission tomography. This type of system exploits FPGAs differential inputs as comparators. In contrast to standard approach [45], where external comparator chips are used, it allows to create more compact and less expensive systems. The process of analog signal comparison in the differential buffer is

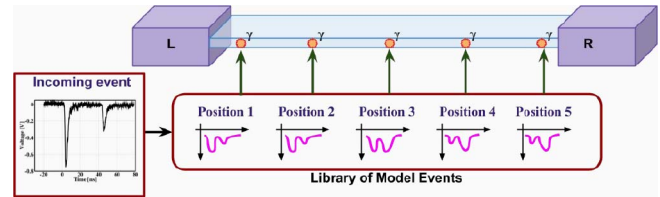


Fig. 5. Schematic representation of the developed reconstruction method. The measured event, consisting of signals registered at both ends of the scintillator is compared to model events determined for a set of well-defined positions along the detector. Orange dots are representing the points of interactions of gamma quanta within the scintillator.

similar to the usage of the standard comparator. On the positive input of an FPGA differential buffer a predefined voltage from data acquisition system (DAQ) is delivered and on the negative side a measured signal. When the signal is crossing the threshold level given by the DAC it creates a transition of digital signal inside the FPGA. This transition corresponds to either a leading or trailing edge and precise times, corresponding to the arrival of these edges, are measured with time to digital converters (TDCs) [46], [47] implemented within FPGA device. It has been shown in [48] that with this approach the intrinsic TDC precision of 20-ps rms per channel is achievable.

III. HIT-POSITION AND HIT-TIME RECONSTRUCTION METHOD FOR LONG PLASTIC SCINTILLATORS

A. Realization of the Method

The proposed reconstruction method, as mentioned earlier, utilizes the signal shape to determine the hit-time and hit-position of photons registered in long scintillating detectors. To this end, the detector is first characterized by determination of signal shapes at a set of well-defined hit positions along the scintillator. Since the signal amplitude can vary even at the same hit position (e.g., due to different energy deposition) we synchronize and average a big statistics of signals at each hit-position which defines so-called model events. Having such a standardized detector the reconstruction is done by comparing the registered event to all the model events stored in a database.

The known hit-time and hit-position of the most similar model event in the database is then treated as the hit-time and hit-position of registered event. In Fig. 5 a schematic illustration of the working principle behind the presented reconstruction method is shown. The Mahalanobis distance formula [49] is used as a measure of similarity between the two compared events. It is a measure of the deviations of the different mean values in terms of the standard deviation in a multivariate analysis. Here, deviation is defined as the correlation between the model and registered events [39].

B. Library of Synchronized Model Events

The library was determined from a scan of scintillator strip with a collimated beam of annihilation photons with profile width of ~ 1.5 mm [50]. The strips were scanned with a step of 3 mm, such that there were in total 98 scanned positions and the information of the irradiated position was obtained by the synchronization of collimator movement with the DAQ [24].

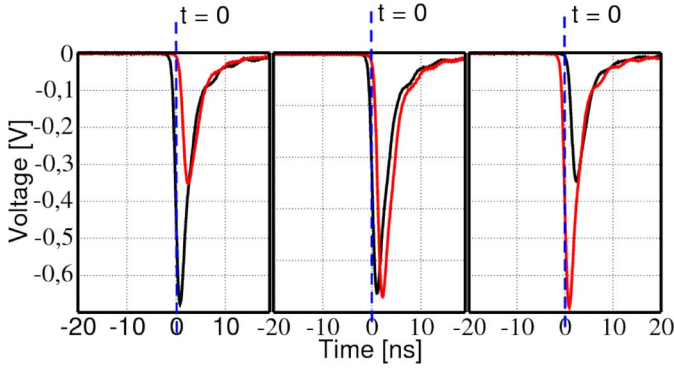


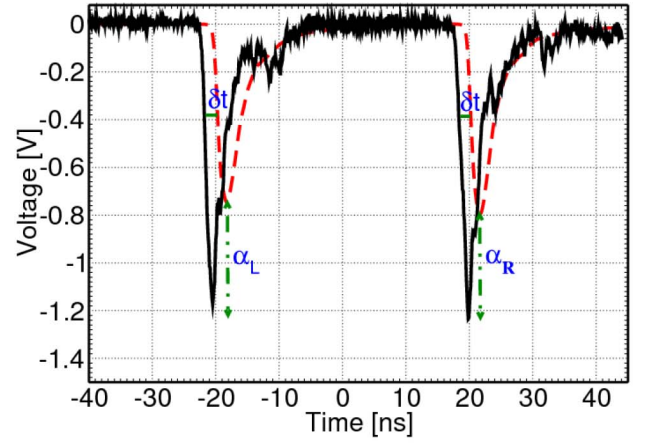
Fig. 6. Example of synchronized signals at three different hit-positions. Solid black and red lines represent signals measured by left and right PM, respectively.

High statistics of events (~ 5000) were collected for each irradiated position. The construction of model signals library was already described in details in [28], here we present only main steps of the procedure comprising.

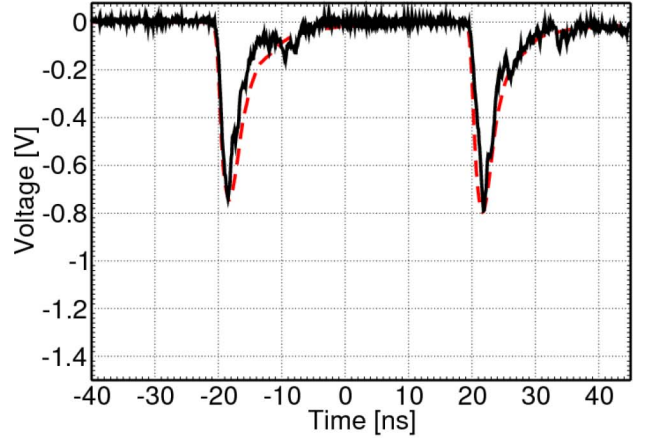
- 1) *Synchronization of Signals*: For each hit-position of photons all the collected events were synchronized in order to have the same hit-time value. This was obtained by using a calibration constant, $t_{\text{synch}} = (t_L + t_R)/2$ for each event, where t_L and t_R are the time values of the left and right ended signals calculated at their beginning point, respectively, and the signals were shifted in time by t_{synch} such that the resulted synchronized signal time is equal to zero as shown in Fig. 6 at three different irradiated positions.
- 2) *Determination of Average Event*: Then averaging over all events for each hit-position was performed and the obtained average event was treated as a reference to align the measured signal as it is shown in Fig. 7(a) and (b).
- 3) *Event's Alignment*: The χ^2 statistics was used for the alignment of signals which is necessary to suppress the spread of the events in terms of amplitude and time

$$\begin{aligned} \chi^2(\delta t, \alpha_L, \alpha_R) &= \sum_{i=1}^n \frac{(t_{\text{AvgLeft}}(V_i) - t_{\text{dbLeft}}(\alpha_L V_i) - \delta t)^2}{n} \\ &+ \sum_{i=1}^m \frac{(t_{\text{AvgRight}}(V_i) - t_{\text{dbRight}}(\alpha_R V_i) - \delta t)^2}{m}. \end{aligned} \quad (1)$$

Here, δt is the shift along the time axis, and α_L and α_R are the normalization factors for signals registered at both ends of the scintillator (left and right, respectively) as shown in Fig. 7(a). $t_{\text{AvgLeft}}(V_i)$ and $t_{\text{AvgRight}}(V_i)$ denote the time of left and right average signals computed for voltage V_i at their leading edge. $t_{\text{dbLeft}}(\alpha_L V_i)$ and $t_{\text{dbRight}}(\alpha_R V_i)$ are the times computed for rescaled left and right signals at their leading edge, respectively [28], [29]. Finally, n and m denote the number of points sampled at the leading edge of the left and right signals, respectively. The set of parameters α_L , α_R , and δt was used for alignment of the measured events for which χ^2 was minimal.



(a)



(b)

Fig. 7. (a) Example of database event before the alignment to average signals. (b) Same database event after the alignment to average signals using α_L , α_R , and δt parameters. Black curve represents measured events while the red one represents computed average events. δt is the shift along the time axis and α_L and α_R are the normalization factors for signals registered at both ends of the scintillator (left and right, respectively).

- 4) *Determination of Model Events Shape*: Afterward an averaging of all the rescaled events was performed resulting in determination of the so-called model event. In Fig. 8 exemplary model events obtained for three different hit-positions are shown.

C. Reconstruction of Hit-Position and Hit-Time

The hit-position of gamma quanta is reconstructed exploiting the Mahalanobis distance [49] as a measure of similarity for two compared events (the measured and the model one), using

$$M.D(z, \Delta t) = \sqrt{\vec{x}(z, \Delta t) C(z)^{-1} \vec{x}(z, \Delta t)^T} \quad (2)$$

where z is the hit-position along the length of the scintillator and Δt denotes the time shift between the two compared events. $\vec{x}(z, \Delta t)$ is a vector whose elements equal to the differences between the elements of the measured and the model event vectors shifted by Δt and $C(z)$ are the covariance matrices. As a result of comparison, only those values of z and Δt were taken into consideration for which minimum value of

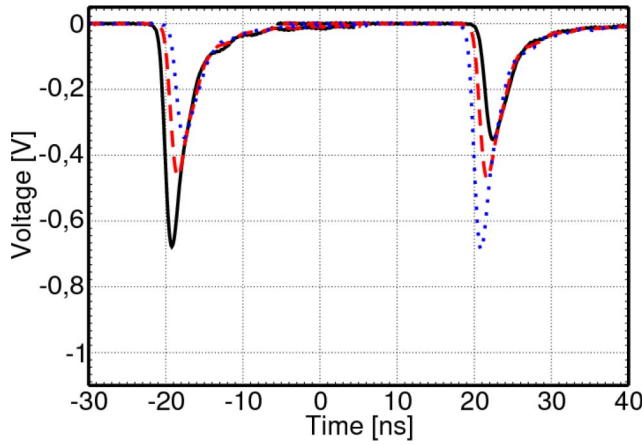


Fig. 8. Exemplary model signals at three different irradiated positions along a strip. Black solid curve shows the model event produced for the position nearest to the left end of the strip. Red dashed curve denotes the model event belonging to the central hit-position and blue dotted curve is the model event for the position lying in the proximity of the right end of the scintillator strip.

the Mahalanobis distance was obtained. The minimum value corresponds to the most similar model event. Formulation of covariance matrices $C(z)$ and $\vec{x}(z, \Delta t)$ vectors was as follows.

- 1) *x-Vector*: The elements of the measured and the model event vectors are the time values calculated at defined set of threshold levels for signals registered at both detector sides. The number of elements in \vec{x} depends on the number of threshold levels applied to the signals of an event. For example, $\vec{x}(z, \Delta t)$ of an event at a single applied threshold level will consist of two elements: one measured from the left- and right-ended PMs connected to the scintillator. It is defined as

$$\vec{x}(z, \Delta t) = \begin{bmatrix} x^L(z, \Delta t) \\ x^R(z, \Delta t) \end{bmatrix} \quad (3)$$

and

$$\begin{aligned} x^L(z, \Delta t) &= t^L - t^{L\text{mod}}(z) - \Delta t \\ x^R(z, \Delta t) &= t^R - t^{R\text{mod}}(z) - \Delta t \end{aligned}$$

where t^L and t^R are the elements of \vec{t} whose values are times at the applied threshold for the left and right signal of measured event, respectively. Similarly, $t^{L\text{mod}}$ and $t^{R\text{mod}}$ are the elements of t^{mod} whose values are the times obtained at the same threshold for model event

$$\begin{aligned} \vec{t} &= [t^L, t^R] \\ t^{\text{mod}} &= [t^{L\text{mod}}, t^{R\text{mod}}]. \end{aligned}$$

- 2) *Covariance Matrix*: The covariance matrix $C(z)$, was computed for each scanned position (mentioned in Section III-B) for the defined set of threshold levels using

$$C_{ij} = \sum_{k=1}^N \frac{(\vec{t}_{k(i)} - \vec{t}_{\text{avg}(i)})(\vec{t}_{k(j)} - \vec{t}_{\text{avg}(j)})}{N} \quad (4)$$

where \vec{t}_k is the vector of times for the k th measured event belonging to the defined hit-position from the scan and \vec{t}_{avg} is the average times vector determined for the

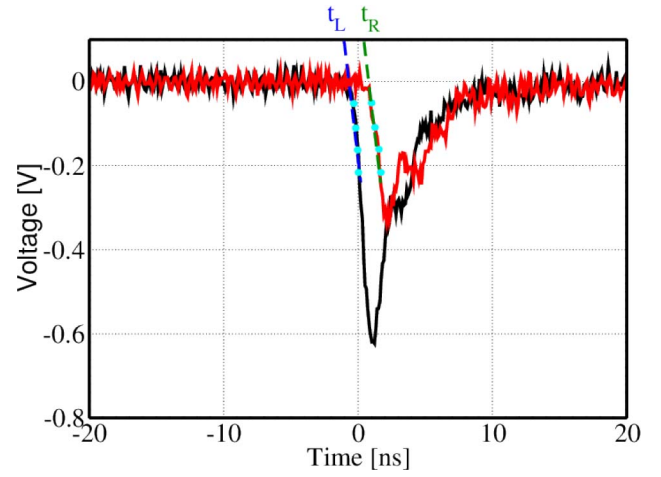


Fig. 9. MVT method applied to a sample event pulse. Black and red curves represent the left and right signals of an event, respectively. Dots are the applied thresholds on both signals. The green and blue dashed lines are lines fitted to leading edges of the left and right signals passing through the applied threshold levels, respectively. The signal times (t_L and t_R) are defined by zero value of the fitted lines and the event time is the average of t_L and t_R (left and right) times.

same hit-position. Indices i and j enumerate the applied threshold levels and N denotes number of events corresponding to the position in the database. The number of elements of the covariance matrix is equal to $(2m)^2$, where m denotes the number of threshold levels applied to the signals.

- 3) *Hit-Time*: Hit-time (interaction time of gamma quanta) is equal to Δt , time shift between the two compared events [51] for minimum Mahalanobis distance obtained from (2). Thus, TOF of annihilation gamma quanta registered in a pair of detectors, denoted A and B, is equal to the difference between hit-times in these detectors and is computed by

$$\text{TOF} = \Delta t_A - \Delta t_B. \quad (5)$$

It is worth to mention that the obtained TOF is independent of the trigger time because the same time affects both detectors. Hence, the proposed method allows direct determination of LOR and TOF.

- 4) *Hit-Position*: Hit-position is the position (z) of most similar model event from the library with respect to measured event for which minimal value of Mahalanobis distance is obtained from (2). This value of (z) is called as the reconstructed hit-position.

IV. LINEAR-FIT METHOD

In this article, in addition to method based on the Mahalanobis distance we also test another method for determining the time of the signals. The second method is based on a linear fit to the times measured at the leading edge analogously as applied in [31], [45], and [52]. The event time was then calculated as a zero value of a regression line fitted to the measured leading edge points. The scheme of the method is shown in Fig. 9.

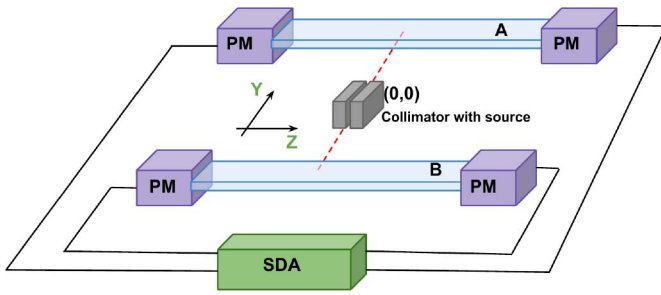


Fig. 10. Schematic view of the double-strip J-PET prototype used for the validation of the proposed method. The two detectors were read out by PMs connected to the Serial Data Analyzer (Lecroy SDA6000A) providing coincident registration of all four signals. A collimated beam of annihilation gamma quanta was provided by a ^{22}Na source placed at (0,0) position.

In [52], this method was tested on the data obtained from a pair of LSO crystals of dimensions $6.25 \times 6.25 \times 25 \text{ mm}^3$. The scintillators were wrapped in the teflon tape and optically coupled to the PM tubes. Signals were readout via a Tektronix TDS6154C digital oscilloscope using coincident technique. A weak ^{18}F source was used to irradiate the scintillators. The signals were sampled at number of predefined voltage levels and the best coincidence timing resolution of about 302 ps (FWHM) was obtained at 16 voltage threshold levels.

In another work [45], using ^{22}Na source, again the signals were sampled at 50, 100, 200, and 300 mV threshold levels and the MVT was used to compute coincidence timing resolution. As a result 340 ps (FWHM) was obtained as coincidence timing resolution which is closer to the value obtained with digital library sampled at 20 GSps using multithreshold discriminator board. Thus, this is also one of the potential methods for implementing digital PET data acquisition.

V. VALIDATION OF THE METHOD

A. Data Collection and Filtration

The method was validated on the same data measured with the double strip J-PET prototype (mentioned in Section III-B). The prototype was built out of two BC-420 [36] plastic scintillators with dimensions $300 \times 19 \times 5 \text{ mm}^3$. Both strips were wrapped with 3M Vikuiti specular reflector foil [53]. Signals from strips were read out using Hamamatsu PMs R9800 [38] connected optically via optical grease EJ-550 to the ends of scintillators and probed by Serial Data Analyzer (Lecroy SDA6000A) with a time interval of 100 ps. The ^{22}Na isotope was used as a source of annihilation photons. For noise suppression only coincident signals from both detectors were registered. The scheme of the used experimental setup is presented in Fig. 10. The measurements were done along the whole length of scintillator at positions for which we earlier determined the library of model signals. This allowed us to determine the achievable performance of the reconstruction in function of the hit position.

After collection of the dataset a primary correction for pedestals was implemented on all the registered signals to have a signal library free of the electronic voltage offset. Next, only those events were considered for the reconstruction of hit-position and hit-time for which energy depositions were

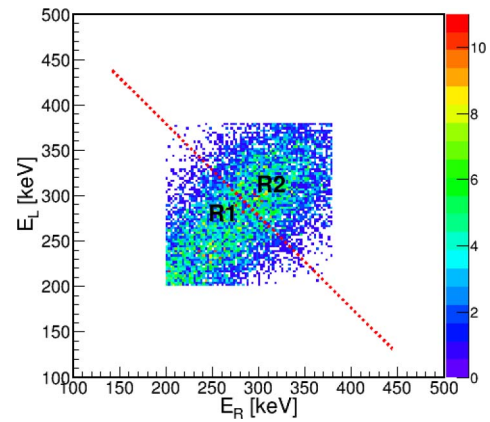


Fig. 11. Scatter plot of energy deposition registered at the left (E_L) and right (E_R) side of one of the J-PET detector modules. The red dotted line shows the bisection of energy loss into 2 parts (R1 and R2) done to improve the TOF resolution. Only energies in the range from 200 keV to 380 keV are shown.

in the range from 200 keV to 380 keV. This is the range of energy loss which will be used for the J-PET tomography in order to minimize the blurring of the image due to the scatterings of gamma quanta in the patient [17], [54]. The relation between the measured charge and deposited energy was computed by fitting the Klein–Nishina formula [55] convoluted with the detector resolution to the experimental energy loss spectrum [17]. The data filtering was done to suppress most of those events which originate from secondary Compton scattering [56] and also from the 1.27-MeV gamma quanta produced in the decay of ^{22}Na isotope.

B. Optimization of the Signal Processing

The full-scale J-PET tomograph signals will be sampled by a dedicated front-end electronics (FEEs) in voltage domain with a predefined set of thresholds with time resolution of about 20 ps [22]. In order to design the optimal configuration of thresholds for the full scale J-PET tomograph it is necessary to determine the optimal number of thresholds and voltage value for each threshold. To this end, the measured data were optimized by constant level discriminator approach followed by energy deposition classifier using the Mahalanobis distance defined in (2). The TOF resolution was used as a criterion for the optimization. We have chosen threshold levels at which root mean squared error value of TOF distribution, i.e., rms (TOF) obtained from Mahalanobis distance is minimal [39]. We have performed tests with a different number of applied threshold levels but no significant improvement was observed on increasing the number of threshold levels by more than two. The reason may be the fact that the signal is composed of many single photoelectron pulses but only few of them contribute significantly to the onset of the leading edge [21].

Thus, we have performed optimization of two-threshold levels for signals measured at the center of the scintillator. As a result, we obtained -55 mV and -100 mV as the optimized constant levels of discrimination and these values were used as the reference for all other hit-positions. It was noticed that the time resolution and, hence, the covariance matrix depends

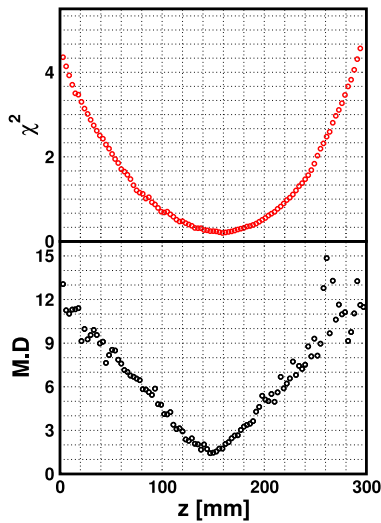


Fig. 12. Position of an event that belongs to the central hit-position, i.e., 150 mm reconstructed by two methods: (upper panel) χ^2 minimization [28] and (lower panel) Mahalanobis distance.

on the number of photoelectrons in the signal which corresponds to the energy deposited by the interacting gamma photon. Therefore, the comparison of signals should improve if the covariance matrix would be established as a function of the energy loss. To check this we divided the range of available energy losses (i.e., 200 keV to 380 keV) into several regions and computed the covariance matrix for each of them separately. No significant improvement in the resolution was found after dividing the whole energy loss region to more than two parts [39]. Bisection of energy distribution into two parts (R1 and R2) is presented in Fig. 11.

VI. RESULTS

A. Mahalanobis Method

The Mahalanobis distance distribution calculated according to (2) for an event from the central hit-position sampled at predefined two-threshold levels are shown in lower panel of Fig. 12. The upper panel of Fig. 12 is showing the χ^2 distribution of the same event presented in [28]. One can see clear the value of position reconstructed by Mahalanobis distance has less uncertainty than the one reconstructed by χ^2 minimization method.

The TOF and spatial resolutions obtained for hit-positions in the range from $(-100, 0)$ mm to $(100, 0)$ mm along the length of scintillator using the Mahalanobis method are presented in Fig. 13(a) and (b), respectively. Exemplary TOF and spatial (Δz) distributions at optimized levels followed by energy classifier are shown in Fig. 14(a) and (b), respectively. It is evident from Fig. 13(a) and (b) that both resolutions remain constant at all z values along the whole length of the scintillator strip. The achieved TOF resolution along 300 mm long scintillator amounts to 325 ps (FWHM) and the spatial resolution is 25 mm (FWHM).

Moreover, in order to test the method in view of its application in positron emission tomography, we performed experiments with bare ^{22}Na sources emitting annihilation gamma quanta isotropically. The activities of the used sources

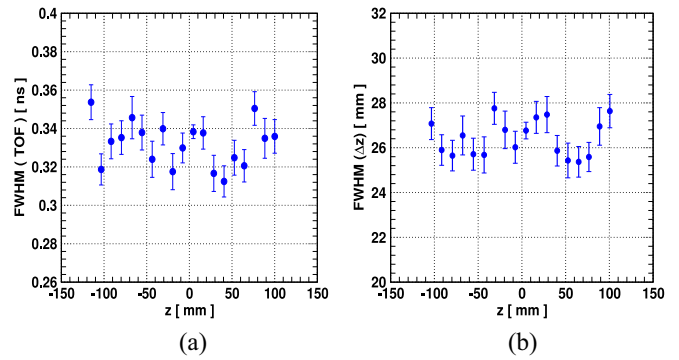


Fig. 13. (a) TOF resolution as a function of the hit-position (z) along the detector. (b) Spatial (Δz) resolution as a function of the hit-position (z) along the detector.

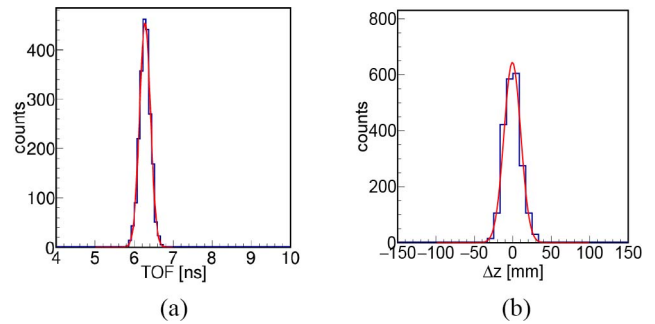


Fig. 14. (a) TOF distribution at the central hit-position with rms (TOF) = 0.138 ± 0.002 ns. The mean of TOF distribution is not zero because of offsets due to different length of cables used to readout the PMs output. (b) Spatial (Δz) distributions at central hit-position with rms (Δz) = 10.7 ± 0.2 mm.

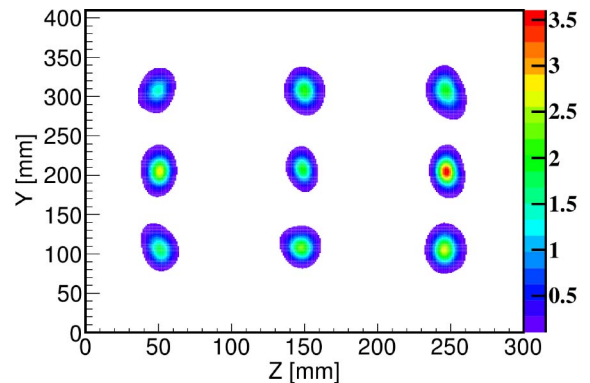


Fig. 15. 2-D image reconstructed for the sources placed at nine different positions using the MLEM algorithm. Each point represents sources of different activity placed in between the two strips. The source at position $(250, 200)$ mm was the most active one.

are listed in Table I. The sources were placed at nine different positions between the two scintillators. The scheme of source position is presented in [39]. The reconstructed image of these sources using maximum likelihood expectation maximization (MLEM) algorithm [57]–[59] is presented in Fig. 15. Even though only two strips were used to detect the signals it was possible to reconstruct a tomographic image. The point spread functions in transverse and axial directions, calculated according to the NEMA norm [60], are equal to $\text{FWHM} = 20.2$ mm and $\text{FWHM} = 7.7$ mm, respectively.

TABLE I
LIST OF DIFFERENT ^{22}Na SOURCES USED FOR THE TEST MEASUREMENT

Source No.	Activity [kBq]
1	393
2	140
3	399
4	391
5	2180
6	11946
7	2185
8	280
9	9

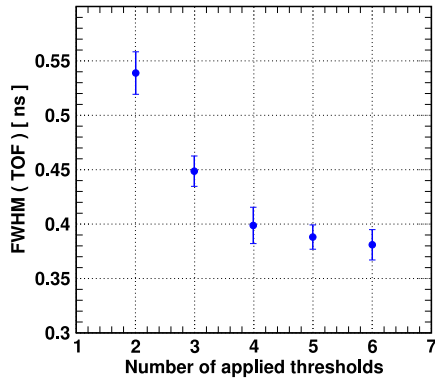


Fig. 16. TOF resolution as a function of the number of applied threshold levels obtained using the linear fitting method. The values of applied thresholds for each set is presented in Table II.

Indeed, the axial and transaxial resolutions obtained for the two-strip J-PET prototype are worse in comparison to commercial tomographs. This was expected, since we have used only one pair of scintillators. However, we expect the further improvement when the image will be done with scintillators forming the cylindrical barrel providing LOR, and TOF in three dimensions [54].

B. Comparison of the Mahalanobis Reconstruction With Linear Fitting Method

In order to test the linear fitting method we have determined the optimal number of applied thresholds looking for the best achievable TOF resolution. The test was performed with different number of threshold levels. For each number of levels different values of threshold were tested, e.g., for two-threshold levels the value of TOF was calculated at a number of different set of values: (-40 mV, -80 mV), (-40 mV, 100 mV), (-60 mV, -100 mV), (-80 mV, -160 mV), etc. In Table II only those values for each number of applied levels are given for which we obtained best TOF resolution. The dependence of TOF resolution on the number of applied threshold levels is shown in Fig. 16. One can see that the resolution improves with the number of applied thresholds, but after discrimination on four of them there is no significant improvement with the current threshold setting in our experiment. The obtained value of rms (TOF) with four predefined threshold levels is comparable with the value calculated using the Mahalanobis method at two predefined threshold levels.

Although the algorithm of the linear fitting method is much easier to apply than the algorithm of the Mahalanobis method,

TABLE II
NUMBER OF APPLIED THRESHOLD LEVELS WITH THEIR VALUES FOR WHICH THE BEST TOF RESOLUTION WAS OBTAINED

Number of applied levels	Values [mV]
2	-40, -80
3	-40, -80, -120
4	-40, -80, -120, -160
5	-40, -80, -120, -160, -200
6	-40, -80, -120, -160, -200, -240
7	-40, -80, -120, -160, -200, -240, 280

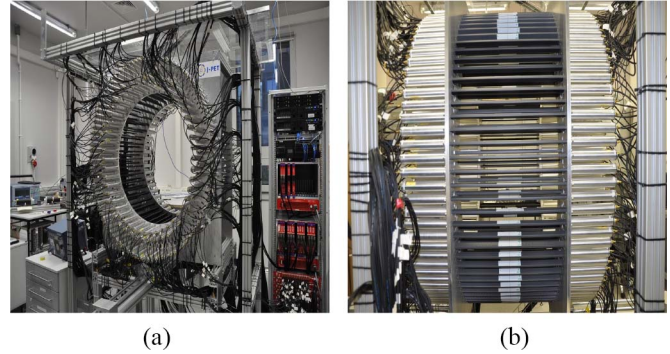


Fig. 17. (a) Front view of the full frame J-PET prototype with large field of view (diameter of 85 cm) and axial length of 50 cm. (b) Rear view of the full frame J-PET prototype with large field of view (diameter of 85 cm) and axial length of 50 cm.

its realization is impractical because it requires four thresholds to achieve the same resolution as with two thresholds when applying the method based on the Mahalanobis distance. A higher number of applied threshold levels would increase the cost of electronics used in the PET scanner and would make it more expensive.

VII. SUMMARY

An optimized method of reconstructing the hit-position and hit-time of photons in scintillator detectors was developed in view of its application for the registration of 511 keV photons in the positron emission tomography. The method was validated on experimental data collected with the double-strip J-PET prototype. It is based on the comparison of the measured signal with synchronized model signals stored in a library utilizing the Mahalanobis distance as a measure of similarity. The reconstructed hit-position of the photons is considered as the position of a library signal most similar to the measured one, and the hit-time is the relative time difference between them. The time difference between the reconstructed hit-time (interaction time) of photons in different detectors corresponds to the TOF which is independent of the trigger time. The best obtained TOF and spatial resolutions amount to 325 ps (FWHM) and 25 mm (FWHM), respectively. This result is comparable to the one obtained from the linear fitting method requiring higher number of predefined thresholds than two.

In summary, the cost of the electronics for a J-PET scanner device depends on the number of voltage thresholds levels needed in the reconstruction of the time and spatial resolution. In this contribution, we have studied two methods and compared them with respect to the obtained resolution. We found

that the Mahalanobis method needs less levels than the linear fitting method in obtaining the same resolution. In a next step, we will apply the Mahalanobis method for all 192 scintillators which build up the J-PET full frame detector positioned along a cylindrical geometry in 3 layers [4]. The front and rear view of the J-PET full frame prototype are shown in Fig. 17(a) and (b), respectively.

ACKNOWLEDGMENT

The authors acknowledge technical and administrative support of A. Heczko, M. Kajetanowicz, and W. Migdał. They are also grateful to Prof. Steven Bass for reading and correcting this article.

REFERENCES

- [1] S. Vandenberghe, E. Mikhaylova, E. D'Hoe, P. Mollet, and J. S. Karp, "Recent developments in time-of-flight PET," *EJNMMI Phys.*, vol. 3, pp. 1–30, Dec. 2016.
- [2] P. J. Slomka, T. Pan, and G. Germano, "Recent advances and future progress in PET instrumentation," *Seminars Nucl. Med.*, vol. 46, pp. 5–19, Jan. 2016.
- [3] J. V. Sluis *et al.*, "Performance characteristics of the digital biograph vision PET/CT system," *J. Nucl. Med.*, vol. 60, pp. 1031–1036, Jul. 2019.
- [4] S. Niedźwiecki *et al.*, "J-PET: A new technology for the whole-body PET imaging," *Acta Physica Polonica B*, vol. 48, no. 10, pp. 1567–1576, 2017.
- [5] P. Moskal *et al.*, "Feasibility study of the positronium imaging with the J-PET tomograph," *Phys. Med. Biol.*, vol. 64, Mar. 2019, Art. no. 055017.
- [6] P. Moskal, B. Jasińska, E. Stepień, and S. D. Bass, "Positronium in medicine and biology," *Nat. Rev. Phys.*, vol. 1, pp. 527–529, Jun. 2019.
- [7] J. L. Lacy, C. S. Martin, and P. L. Armendarez, "High sensitivity, low cost PET using Lead-walled straw detectors," *Nucl. Instrum. Methods Phys. Res. A, Accelerators Spectrometers Detectors Assoc. Equip.*, vol. 471, pp. 88–93, Sep. 2001.
- [8] N. N. Shehad, A. Athanasiades, C. S. Martin, L. Sun, and J. L. Lacy, "Novel lead-walled straw PET detector for specialized imaging applications," in *Proc. IEEE Nucl. Sci. Symp. Conf. Rec.*, vol. 5, Fajardo, Puerto Rico, 2005, pp. 2895–2898.
- [9] G. Belli *et al.*, "RPC: From high energy physics to positron emission," *J. Phys. Conf. Series*, vol. 41, May 2006, pp. 555–560.
- [10] A. Blanco *et al.*, "Efficiency of RPC detectors for whole-body human TOF-PET," *Nucl. Instrum. Methods Phys. Res. A, Accelerators Spectrometers Detectors Assoc. Equip.*, vol. 602, pp. 780–783, May 2009.
- [11] I. Vilardi *et al.*, "Optimization of the effective light attenuation length of YAP:Ce and LYSO:Ce crystals for a novel geometrical PET concept" *Nucl. Instrum. Methods Phys. Res. A, Accelerators Spectrometers Detectors Assoc. Equip.*, vol. 564, pp. 506–514, Aug. 2006.
- [12] C. Casella, M. Heller, C. Joram, and T. Schneider, "A high resolution TOF-PET concept with axial geometry and digital SiPM readout," *Nucl. Instrum. Methods Phys. Res. A, Accelerators Spectrometers Detectors Assoc. Equip.*, vol. 736, pp. 161–168, Feb. 2014.
- [13] S. R. Cherry, T. Jones, J. S. Karp, J. Qi, W. Moses, and R. Badawi, "Total-body PET: Maximizing sensitivity to create new opportunities for clinical research and patient care," *J. Nucl. Med.*, vol. 58, pp. 3–11, Jan. 2018.
- [14] V. Viswanath *et al.*, "Development of PET for total-body imaging," *Acta Physica Polonica B*, vol. 48, no. 10, pp. 1555–1566, 2017.
- [15] S. R. Cherry, R. D. Badawi, J. S. Karp, W. W. Moses, P. Price, and T. Jones, "Total-body imaging: Transforming the role of positron emission tomography," *Sci. Transl. Med.*, vol. 9, pp. 1–3, Mar. 2017.
- [16] P. Moskal, P. Salabura, M. Silarski, J. Smyrski, J. Zdebik, and M. Zieliński, "Novel detector systems for the positron emission tomography," *Bio Algorithms Med Syst.*, vol. 7, no. 2, pp. 73–78, 2011.
- [17] P. Moskal *et al.*, "Test of a single module of the J-PET scanner based on plastic scintillators," *Nucl. Instrum. Methods Phys. Res. A, Accelerators Spectrometers Detectors Assoc. Equip.*, vol. 764, pp. 317–321, Nov. 2014.
- [18] P. Moskal *et al.*, "A novel method for the line-of-response and time-of-flight reconstruction in TOF-PET detectors based on a library of synchronized model signals," *Nucl. Instrum. Methods Phys. Res. A, Accelerators Spectrometers Detectors Assoc. Equip.*, vol. 775, pp. 54–62, Mar. 2015.
- [19] P. Moskal, "A method and a system for determining parameters of reactions of gamma quanta within scintillation detectors of PET scanners," Patent EP2454612, 2014.
- [20] J. Smyrski *et al.*, "Measurement of gamma quantum interaction point in plastic scintillator with WLS strips," *Nucl. Instrum. Methods Phys. Res. A, Accelerators Spectrometers Detectors Assoc. Equip.*, vol. 851, pp. 39–42, Apr. 2017.
- [21] P. Moskal *et al.*, "Time resolution of the plastic scintillator strips with matrix photomultiplier readout for J-PET tomograph," *Phys. Med. Biol.*, vol. 61, pp. 2025–2047, Feb. 2016.
- [22] M. Pałka *et al.*, "A novel method based solely on field programmable gate array (FPGA) units enabling measurement of time and charge of analog signals in positron emission tomography (PET)," *Bio Algorithms Med Syst.*, vol. 10, no. 1, pp. 41–45, 2014.
- [23] M. Pałka *et al.*, "Multichannel FPGA based MVT system for high precision time (20 ps RMS) and charge measurement," *J. Instrum.*, vol. 12, pp. 1–10, Aug. 2017.
- [24] G. Korcyl *et al.*, "Sampling FEE and trigger-less DAQ for the J-PET scanner," *Acta Physica Polonica B*, vol. 47, pp. 491–496, Feb. 2016.
- [25] G. Korcyl *et al.*, "Evaluation of single-chip, real-time tomographic data processing on FPGA SoC devices," *IEEE Trans. Med. Imag.*, vol. 37, no. 11, pp. 2526–2535, Nov. 2018.
- [26] L. Raczyński *et al.*, "Novel method for hit-position reconstruction using voltage signals in plastic scintillators and its application to positron emission tomography," *Nucl. Instrum. Methods Phys. Res. A, Accelerators Spectrometers Detectors Assoc. Equip.*, vol. 764, pp. 186–192, Nov. 2014.
- [27] L. Raczyński *et al.*, "Compressive sensing of signals generated in plastic scintillators in a novel J-PET instrument," *Nucl. Instrum. Methods Phys. Res. A, Accelerators Spectrometers Detectors Assoc. Equip.*, vol. 786, pp. 105–112, Jun. 2015.
- [28] P. Moskal *et al.*, "Hit time and hit position reconstruction in the J-PET detector based on a library of averaged model signals," *Acta Physica Polonica A*, vol. 127, pp. 1495–1499, Feb. 2015.
- [29] N. G. Sharma *et al.*, "Reconstruction of hit-time and hit-position of annihilation quanta in the J-PET detector using the Mahalanobis distance," *Nukleonika*, vol. 60, pp. 765–769, Aug. 2015.
- [30] L. Raczyński *et al.*, "Calculation of the time resolution of the J-PET tomograph using kernel density estimation," *Phys. Med. Biol.*, vol. 62, pp. 5076–5097, Jun. 2017.
- [31] Q. Xie, C. Kao, Z. Hsiau, and C. Chen, "A new approach for pulse processing in positron emission tomography," *IEEE Trans. Nucl. Sci.*, vol. 52, no. 4, pp. 988–995, Aug. 2005.
- [32] D. Zhenzhou and Q. Xie, "Quadratic programming time pickoff method for multivoltage threshold digitizer in PET," *IEEE Trans. Nucl. Sci.*, vol. 62, no. 3, pp. 805–813, Jun. 2015.
- [33] D. Zhenzhou, P. Xiao, and Q. Xie, "Event pulse classification with multivoltage threshold samples for scatter rejection in PET," in *Proc. IEEE Nucl. Sci. Symp. Med. Imag. Conf.*, Seattle, WA, USA, 2016, pp. 1–3.
- [34] *Scinnox Organic Scintillators*. Accessed: Mar. 30, 2019. [Online]. Available: <http://scinnox.nl/frame/>
- [35] M. Battablieri. *Scintillation Detectors*. Accessed: Mar. 30, 2019. [Online]. Available: <https://www.ge.infn.it/~batta/Lect1-scint.pdf>
- [36] *Saint Gobain Crystals*. Accessed: Mar. 30, 2019. [Online]. Available: <http://www.crystals.saint-gobain.com>
- [37] R. Mao, L. Zhang, and R. Y. Zhu, "Optical and scintillation properties of inorganic scintillators in high energy physics," *IEEE Trans. Nucl. Sci.*, vol. 55, no. 4, pp. 2425–2431, Aug. 2008.
- [38] (2010). *Hamamatsu-Corporation*. [Online]. Available: <http://sales.hamamatsu.com/en/products/electron-tubedivision/detectors/photomultiplier-tubes.php>
- [39] N. G. Sharma, "Hit-time and hit-position reconstruction of gamma quanta in the J-PET tomography system based on a library of model signals," Ph.D. dissertation, Dept. Exp. Partic. Phys. Appl., Jagiellonian Univ., Kraków, Poland, 2018. [Online]. Available: <http://koza.if.uj.edu.pl/files/3bf9775d2ed55e1deb7dee9a187f6a20/thesis.pdf>
- [40] D. Xi, C.-M. Kao, W. Liu, C. Zheng, X. Liu, and Q. Xie, "FPGA-only MVT digitizer for TOF PET," *IEEE Trans. Nucl. Sci.*, vol. 60, no. 5, pp. 3253–3261, Oct. 2013.
- [41] D. Xi *et al.*, "A PET detector module using FPGA-only MVT digitizers," in *Proc. IEEE Nucl. Sci. Symp. Med. Imag. Conf. (NSS/MIC)*, vol. 10, Seoul, South Korea, 2013, pp. 1–5.

- [42] J. Y. Won and J. S. Lee, "Highly integrated FPGA-only signal digitization method using single-ended memory interface input receivers for time-of-flight PET detectors," *IEEE Trans. Biomed. Circuits Syst.*, vol. 12, no. 6, pp. 1401–1409, Dec. 2018.
- [43] J. Y. Won, S. I. Kwon, H. S. Yoon, G. B. Ko, J. W. Son, and J. S. Lee, "Dual-phase tapped-delay-line time-to-digital converter with on-the-fly calibration implemented in 40 nm FPGA," *IEEE Trans. Biomed. Circuits Syst.*, vol. 10, no. 1, pp. 231–242, Feb. 2016.
- [44] J. Y. Won and J. S. Lee, "Time-to-digital converter using a tuned-delay line evaluated in 28-, 40-, and 45-nm FPGAs," *IEEE Trans. Instrum. Meas.*, vol. 65, no. 7, pp. 1678–1689, Jul. 2016.
- [45] H. Kim *et al.*, "A multi-threshold sampling method for TOF-PET signal processing," *Nucl. Instrum. Methods Phys. Res. A, Accelerators Spectrometers Detectors Assoc. Equip.*, vol. 602, pp. 618–621, Apr. 2009.
- [46] J. Kalisz, R. Szplet, J. Pasierbinski, and A. Poniecki, "Field-programmable-gate-array-based time-to-digital converter with 200-ps resolution," *IEEE Trans. Instrum. Meas.*, vol. 46, no. 1, pp. 51–55, Feb. 1997.
- [47] J. Wu and Z. Shi, "The 10-ps wave union TDC: Improving FPGA TDC resolution beyond its cell delay," in *Proc. Nucl. Sci. Symp. Conf. Rec.*, vol. 10. Dresden, Germany, 2008, pp. 3440–3446.
- [48] A. Neisera *et al.*, "TRB3: A 264 channel high precision TDC platform and its applications," *J. Instrum.*, vol. 8, Dec. 2013, Art. no. C12043.
- [49] P. C. Mahalanobis, "On the generalized distance in statistics," *Proc. Nat. Inst. Sci. India*, vol. 2, no. 1, pp. 49–55, 1936.
- [50] E. Kubicz *et al.*, "Beam profile investigation of the new collimator system for the J-PET detector," *Acta Physica Polonica B*, vol. 47, pp. 537–548, Feb. 2016.
- [51] P. Moskal, "A method and a system for determining parameters of reactions of gamma quanta within scintillation detectors of PET scanners," Patent PL 228119, U.S. 10 088 581, 2018.
- [52] Q. Xie *et al.*, "Potentials of digitally sampling scintillation pulses in timing determination in PET," *IEEE Trans. Nucl. Sci.*, vol. 56, no. 5, pp. 2607–2613, Oct. 2009.
- [53] *3M Optical Systems/Vikuiti*. Accessed: Mar. 30, 2019. [Online]. Available: www.3M.com/Vikuiti
- [54] P. Kowalski *et al.*, "Estimating the NEMA characteristics of the J-PET tomograph using the GATE package," *Phys. Med. Biol.*, vol. 63, Aug. 2018, Art. no. 165008.
- [55] O. Klein and Y. Nishima, "Über die streuung von strahlung durch freie elektronen nach der neuen relativistischen quantendynamik von dirac," *Z. Physik*, vol. 52, pp. 853–868, Nov. 1929.
- [56] P. Kowalski *et al.*, "Scatter fraction of the J-PET tomography scanner," *Acta Physica Polonica B*, vol. 47, pp. 549–560, Feb. 2016.
- [57] A. Słomski *et al.*, "3D PET image reconstruction based on maximum likelihood estimation method (MLEM) algorithm," *Bio-Algorithms Med Syst.*, vol. 10, no. 1, pp. 1–7, 2014.
- [58] P. Białaś *et al.*, "GPU accelerated image reconstruction in a two-strip J-PET tomograph," *Acta Physica Polonica A*, vol. 127, pp. 1500–1504, Feb. 2015.
- [59] A. Strzelecki, "Image reconstruction and simulation of strip positron emission tomography scanner using computational accelerators," Ph.D dissertation, Dept. Inst. Fundam. Technol. Res., Polish Acad. Sci., Warsaw, Poland, 2016.
- [60] *Performance Measurements of Positron Emission Tomographs*, Standard NEMA NU 2-2012, 2012.